Journal of the European Ceramic Society 20 (2000) 1215–1224

# Toughness-curve behaviour of alumina-SiC and ZTA-SiC composites

Henryk Tomaszewski*, Marek Boniecki, Helena Weglarz

*Institute of Electronic Materials Technology, Wólcyńska 133, 01-919 Warsaw, Poland*

Received 1 June 1999; received in revised form 14 September 1999; accepted 8 October 1999

**Abstract**

The fracture behaviour of alumina and ZTA matrix ceramics containing 10–30 wt% SiC particles was investigated during controlled crack growth using three point bending tests of single-edge-notched samples. The crack was initiated and slowly grown by repeated loading and removing of the load. The crack length, $c$, was measured by in-situ observation using a special video camera. The necessary force, $P$, responsible for a crack length increase was recorded by computer control of the testing machine. From the crack length, $c$, and the applied force, $P$, the stress intensity factor, $K_I$, was calculated. The tests showed that SiC addition strongly decreases the $R$-curve effect in alumina and ZTA ceramics. This phenomenon was explained by analysis of the residual stress state in the ceramics. An increased resistance to crack initiation as well as to fracture with increase of SiC addition was also found for the studied ceramics. 

*Keywords:* $Al_2O_3$; Composites; SiC; Toughening; $Al_2O_3$–SiC

## 1. Introduction

Normally the toughness-curve ($T$- or $R$-curve) behaviour is characterized by a change, usually showing an increase in toughness due to material's resistance to crack propagation with crack extension. In many brittle solids it originates from crack tip shielding mechanisms that operate in the crack wake, exerting a crack closure force that decreases the net stress intensity at the crack tip. The $R$-curve results from the accumulation of this closure force with crack growth, typically reaching a saturation limit. It is well established that the $R$-curve behaviour of alumina is due to the formation of frictional tractions (grain bridges) between opposing crack faces in the crack wake.[1] Microstructure variables that are known to control the level of toughening achievable via this mechanism include grain size and shape as well as the magnitude of internal stresses[2] originating from the combination of elastic modulus and thermal mismatch.

Grain size and shape dictate the critical crack opening displacement above which grain bridges disengage and hence, in part, the length of the bridged wake. In this manner, the frictional energy dissipated during crack face separation is enhanced. Internal residual stresses are believed to control the bridge-restraining stress, which in turn dictates the amount of frictional energy dissipated during bridge pull-out and therefore the toughening contribution and $R$-curve enhancement. The residual stresses may be enhanced by the addition of the second phase whose thermal expansion coefficient shows the desired degree of mismatch with that of the matrix. The mechanical behaviour of such two-phase composites have been studied by several workers.[3–5] The importance of the role of residual stresses in increased crack growth resistance of particulate-reinforced ceramic matrix composites was demonstrated by Virkar and Johnson[6] and Taya et al.[7] The periodic residual stress model was used to explain the toughness increase which was observed in the $ZrO_2$-Zr composite.[6] The model proposed by Evans et al[8] and Cutler and Virkar [9] provided the fracture toughness, $K_{Ic}$, of a particulate composite due to periodic residual stress field as

$$K_{Ic} = K_{I0} + 2q\sqrt{\frac{2D}{\pi}} \quad (1)$$

* Corresponding author. Tel.: +4822-83530441; fax: +48-22-8349003.
*E-mail address:* tomasz-h@sp.itme.edu.pl (H. Tomaszewski).

0955-2219/00/$ - see front matter 
PII: S0955-2219(99)00273-3

where $K_{I0}$ is the critical stress intensity factor of the matrix, $q$ is the local residual compressive stress, and $D$ is the length of the compressive stress zone which in this case is the average particulate spacing.

Eq. (1) is based on a stress intensity factor solution by Tada et al.[10] for a semi-infinite two-dimensional crack with a compressive stress zone of intensity $q$ and length $D$. The compressive thermal residual stress in the matrix is generated when the thermal expansion coefficient of the particulate exceeds that of the matrix. This was the case with the $TiB_2$-particulate/SiC matrix composite analysed by Taya et al.[7] They modified Eq. (1) to

$$\Delta K_I = 2q\sqrt{\frac{2(\lambda - d)}{\pi}} \tag{2}$$

where $\lambda$ is an interparticulate distance and $d$ is an average diameter of particulates. Eq.(2) is valid also for the tensile residual stress, $q$, in which case a reduction in $K_{Ic}$ is expected. In the present study the effect of SiC grain addition (a phase with lower thermal expansion coefficient — $\alpha_{SiC} = 3.5\text{–}4.2\times10^{-6}\ °C^{-1}$, $\alpha_{Al_2O_3} = 9.0\times10^{-6}\ °C^{-1}$) on residual stress state change in alumina and ZTA (zirconia toughened alumina) matrices, and the resulting altered crack behaviour were investigated. In comparison to the work of Virkar and Johnson[6] and of Taya et al.,[7] where residual stresses were calculated, in our case they were measured by means of the piezospectroscopic technique. As expected, SiC addition resulted in the development of residual tensile stresses in the ceramic matrices and in turn to the reduction of the effectiveness of the grain bridging mechanism leading to a decrease of the $R$-curve behaviour.

## 2. Experimental procedure

Two types of ceramic matrix were used in this study. The first one was an alumina of the following chemical composition: $Al_2O_3$ — 99.55wt%, MgO — 0.20 wt%, $Y_2O_3$ — 0.25wt%. The alumina powder was high purity (4N concentration) with an average grain size below 0.5μm. The second matrix was a ZTA ceramic prepared by adding 10 wt% zirconia, obtained by using chemical methods,[12] to the above mentioned alumina mixture. The starting SiC powder was β-phase with an average particle size about 1μm. Matrix powders were mixed with SiC (0–30 wt%) in ethanol and then hot-pressed in carbon dies lined with BN layers under a pressure of 15 MPa and a temperature of 1700°C for 1 h in argon atmosphere. The hot pressed specimens were cut and ground yielding bars having the dimensions of 4×4×40 mm (square) or 1.5×6×40 mm (rectangular), and one surface was polished. In the central part of the rectangular bar samples (1.5×6×40) a sharp notch was prepared for testing the crack propagation behaviour.[13] The polished surface of the samples was covered with a 150 nm thick Al layer to improve the crack path visibility during the test.

To verify the contribution of the change in $Al_2O_3$ grain size in the $R$-curve properties of alumina and ZTA matrices with SiC particles addition, samples of pure alumina matrices having different grain sizes were prepared. In this case the alumina matrix powder was cold pressed under 140 MPa and sintered at 1350–1900°C for 1–20 h in a vacuum furnace.

The bending strength of the composites was determined on square bars having the dimensions 4×4×40 mm in a three-point bending test using a universal testing machine (Model 1446, Zwick) with 1 mm/min loading speed and 36.5 mm bearing distance.

For measurements of Young's modulus the beams were thinned to the height of 1 mm and then the compliance of the samples was recorded during loading tests with 0.1 mm/min loading speed and 36.5 mm bearing distance. The values of Young's modulus were determined using the relationship given by Fett and Munz,[14] which is stated in Eq. (5) below.

The controlled crack growth tests were performed during three-point bending with 1μm/min loading speed and 36.5 mm bearing distance using the same testing machine. The crack was initiated and slowly grown by repeated loading and unloading. The crack length $c$ was measured in situ using a special device, consisting of a horizontal light microscope coupled with a CCD camera, which were fitted to the testing machine by a system of elevator stages driven by stepping motors. This enables the precise movement of the microscope objective in $x$-$y$-$z$ directions for adjustment, focussing and tracking on the beam side and bottom surface where the crack propagated. A measuring and picture registration system (framegrabber) was coupled with the load and strain system of the testing machine, and both systems were controlled by a computer. The optical and electronic magnifications were about 250x. Typical paths of a crack propagated in an alumina matrix and registered by the computer are shown in Fig. 1. The stress intensity factor, $K_I$, was calculated from crack length, $c$, and force, $P$.

In several samples the crack growth tests were done without unloading. The time dependent displacement, $d$, of the sample was measured and recorded together with values of force, $P$. According to Fett and Munz,[14] the total compliance, $C$, which is given by Eq.(3)

$$C = \frac{d}{P} \tag{3}$$

consists of the compliance of the measuring system, $C_u$, the compliance of the uncracked bar, $C_0$, and the portion $\Delta C$ caused by the crack:

$$C = C_u + C_0 + \Delta C \tag{4}$$

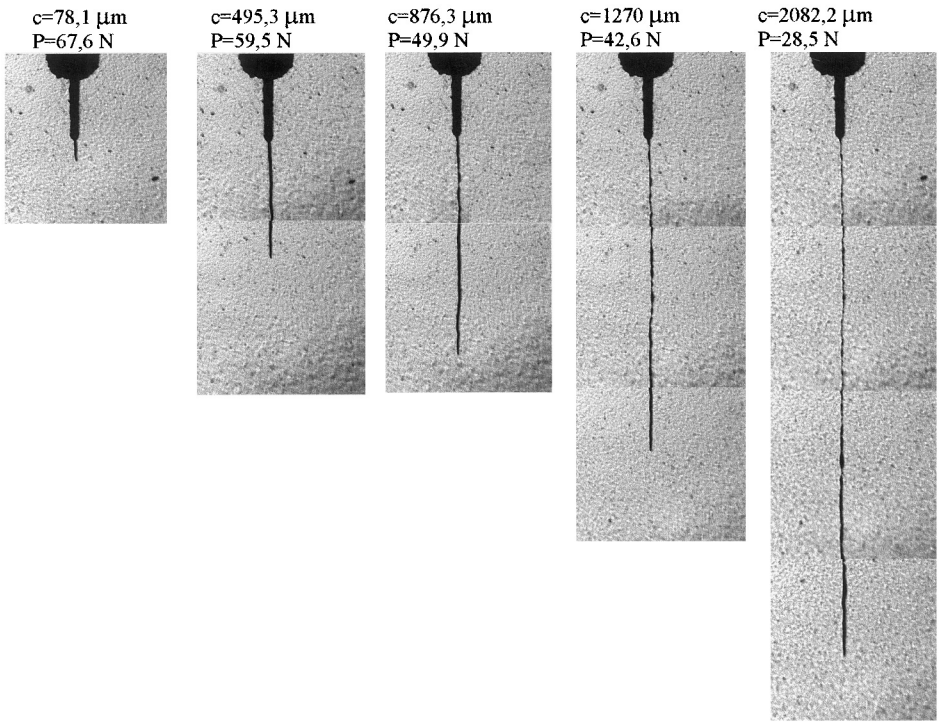


Fig. 1. An example of the consecutive steps of crack propagation in an alumina matrix registered by computer. Above the images the applied force $P$ and the length $c$ of the generated crack are listed.

with

$$C_0 = \frac{L^2}{w^2 BE}\left[\frac{L}{4w} + (1+\nu)\frac{w}{2L}\right] \tag{5}$$

where $E$ is Young's modulus, $\nu$ is Poissons ratio, $w$ is the specimen thickness, $B$ is the specimen width and $L$ is the bearing distance. The compliance part due to the crack was obtained from Ref. 14 as

$$\Delta C = 4.5\frac{L^2}{w^2 EB}\left(\frac{a}{1-a}\right)^2 \sum_{i=0}^{5}\sum_{j=0}^{3} B_{ij} a^i \left(\frac{w}{L}\right)^j \tag{6}$$

with

$$a = \frac{c}{w},$$

where $c$ is the length of the crack and $B_{ij}$ are the coefficients given by Fett and Munz.[14] The stress intensity factor, $K_I$, has been determined from the relation (7)

$$K_I = 1.5\frac{PL}{w^2 B} Y c^{\frac{1}{2}} \tag{7}$$

using the geometric function, $Y$, stated below in Eq. (8), using the coefficients, $A_{ij}$, given by Fett and Munz [14].

$$Y = \frac{\sqrt{\Pi}}{(1-a)^{3/2}}\left[0.3738a + (1-a)\sum_{i,j=0}^{4} A_{ij} a^i \left(\frac{w}{L}\right)^j\right] \tag{8}$$

By this procedure the maximal stress intensity factor, $K_{\mathrm{Imax}}$, and the resistance to crack initiation, $K_{\mathrm{Ii}}$, were calculated. The crack growth rate $v = dc/dt$, controlled by the stress intensity factor, $K_I$, was calculated from the time dependence of the crack length $c$. Assuming a power-law relation between $v$ and $K_I$

$$v = \frac{\mathrm{d}c}{\mathrm{d}t} = AK_I^n \tag{9}$$

the parameters $n$ and $A$ (or $\log A$) were obtained.

Residual stresses within the studied alumina matrix of composites were measured using the piezospectroscopic technique described in detail in publications.[13,15] An optical microscope was used to both excite the fluorescence and to collect and analyse the resulting fluorescence spectrum using an attached spectrometer (DILOR X4800). The 514.5 nm line of an argon ion laser was used to excite the fluorescence. The fluorescence signals were collected from a region of about 50 μm diameter in size. The intensity of the $R_1$ and $R_2$ fluorescence lines were scanned by integrating over 0.5 s intervals at a spacing of 0.2 wavenumbers with the intensity being recorded under computer control. The collected data were subsequently analysed with curve-fitting algorithms

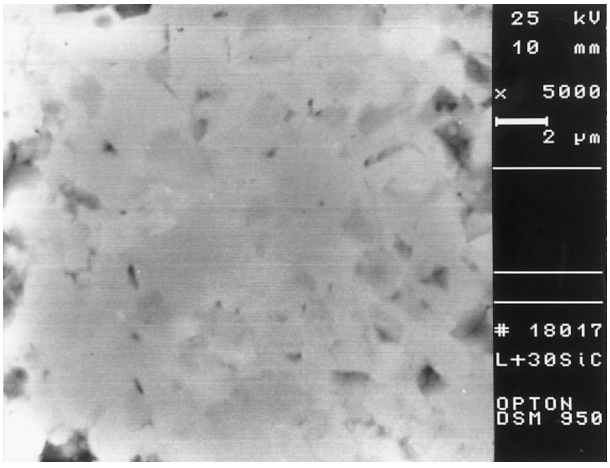


Fig. 2. Secondary-electron image of a polished, non-etched surface of an alumina matrix with 30 wt% SiC (SiC grains — more gray fields).

(double Lorentz function). The line position was indentified by simultaneously fitting the $R_1$ and $R_2$ peaks using the NiceFit software package. All measurements were performed at room temperature. The peak shift due to temperature fluctuation was corrected using the ruby calibration. The instrumental shift was also corrected by simultaneously monitoring a characteristic Neon line at 14564 $cm^{-1}$. The average residual stress in the alumina matrix was calculated from the measured frequency shifts according to a relation of linear proportionality through the average piezospectroscopic coefficients given by He and Clarke.[17]

Microstructural observations of the composites under study, were performed on polished surfaces of the samples by SEM using an OPTON DSM 950 microscope. A typical microstructure of an alumina matrix with 30 wt% SiC addition is shown in Fig. 2. Grain size measurements

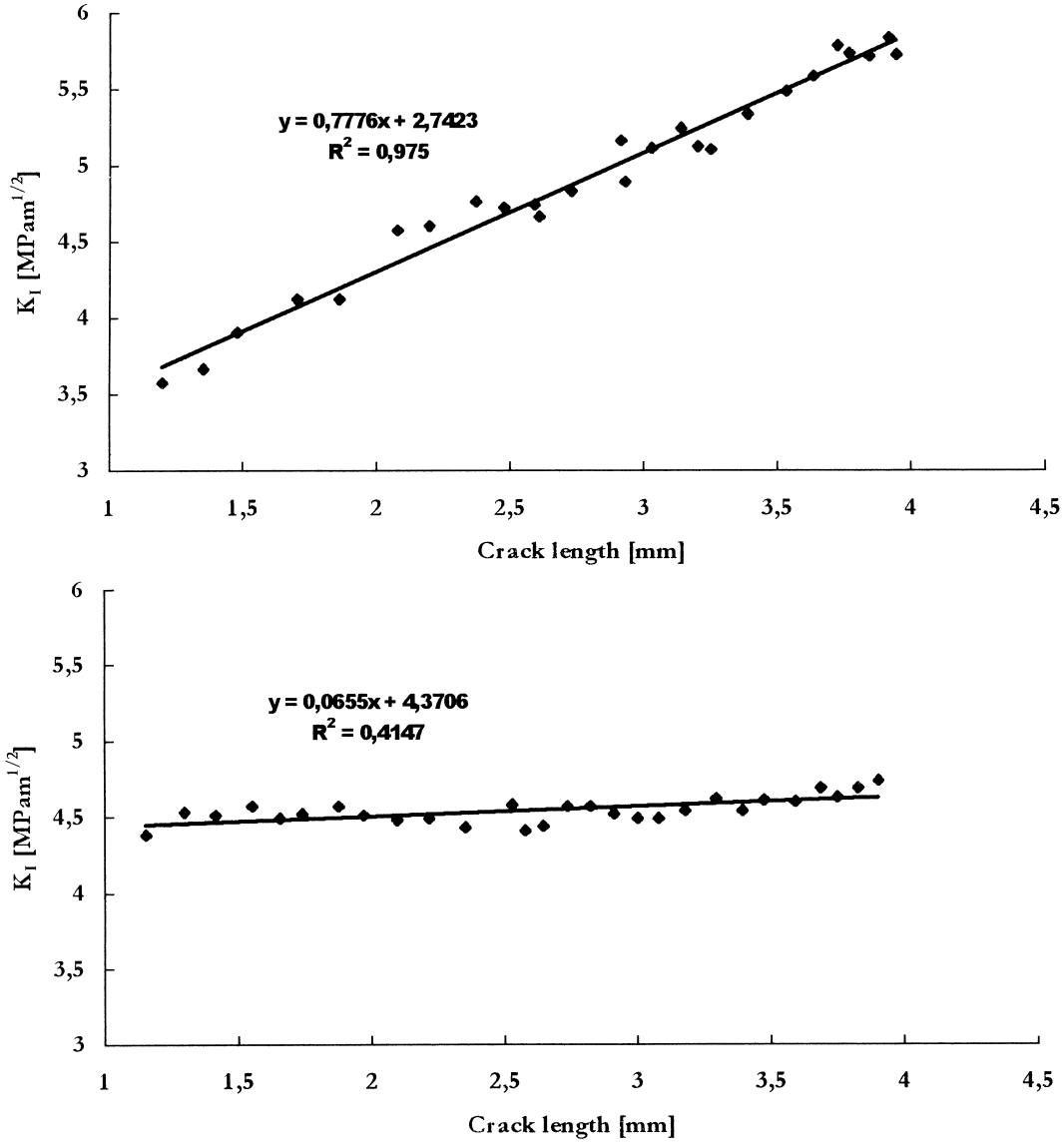


Fig. 3. Dependence of $K_I$ on the crack length for an alumina matrix without SiC (top) and for 30 wt% SiC content (bottom).

were made using samples that were first polished and then thermally etched at 1450°C in argon atmosphere.

## 3. Results and discussion

Figs. 3 and 4 show the data of $K_I = f(c)$ obtained in the range of crack length studied, fitted by a linear equation of $y = ax + b$. The slope, $a$, can be used as a factor describing the tendency of a ceramic towards $R$-curve behaviour. The dependency of the parameters $a$ and $b$ on SiC content for various alumina and ZTA matrices is listed in Table 1. The value of $a$ for a pure alumina matrix is 0.851, which means that the toughness increases strongly namely from 3.6 to about 5.8 $MPam^{1/2}$ as the crack length increases up to 4.0 mm (see Fig. 3). The increase in toughness becomes less pronounced as the SiC content increases. For a SiC content of 30 wt% in an alumina matrix, the slope parameter decreases almost to zero. A similar tendency is observed in the ZTA matrix (Fig. 4 and Table 1). However, the decrease of $R$-curve properties with increasing SiC content is smaller than in the case of the alumina matrix.

Table 1
Linear coefficients $a$ and $b$ (equation of $y = ax + b$) for alumina and ZTA matrices as a function of SiC content

| SiC content (wt%) | Alumina | | ZTA | |
|---|---|---|---|---|
| | $a$ | $b$ | $a$ | $b$ |
| 0 | 0.851 ± 0.074 | 2.64 ± 0,09 | 0.322 ± 0.115 | 3.91 ± 0.08 |
| 10 | 0.378 ± 0.025 | 3.88 ± 0.08 | 0.234 ± 0.034 | 4.44 ± 0.10 |
| 20 | 0.224 ± 0.007 | 4.02 ± 0.02 | 0.112 ± 0.024 | 5.05 ± 0.07 |
| 30 | 0.061 ± 0.024 | 4.44 ± 0.11 | 0.155 ± 0.023 | 4.60 ± 0.09 |

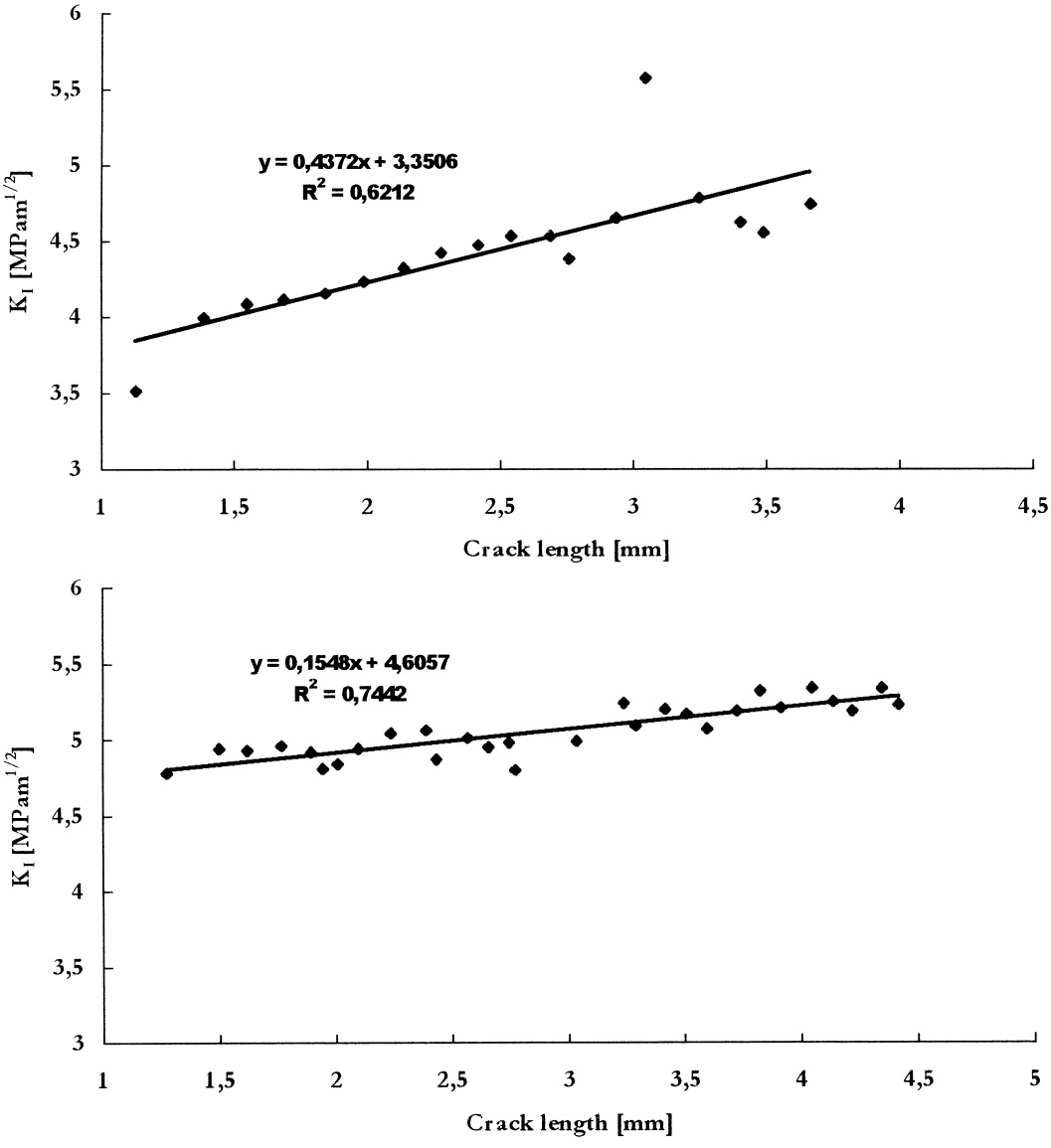


Fig. 4. Dependence of $K_I$ on the crack length for a ZTA matrix without SiC (top) and for 30 wt% SiC content (bottom).

In both cases, the negative effect of SiC addition on the *R*-curve behaviour can be related to the change of the residual stress state. As it was said earlier, due to crystallographic and thermal anisotropy of alumina, some grains in the alumina matrix are subjected to compression and play the role of "bridges". The remaining grains subject to tension are considered as making up the constitutive "matrix". According to Bennison et al.,[1] the bridging grains wedged in the microstructure by these internal compressive stresses lead to an increase in fracture toughness as the crack grows. The addition of SiC particles is expected to change the described stress state. The large thermal expansion mismatch between SiC particles and the $Al_2O_3$ matrix is thought to create additional regions of tension, which has been confirmed by piezo-spectroscopic measurements. As can be seen from Table 2, an increasing content of SiC grains changes the residual stresses in both matrices from compressive to tensile. This in turn reduces the effectiveness of grain bridging and, in consequence, the value of the slope parameter *a*. The smaller decrease of *a* with increasing SiC content observed in ZTA matrix seems to be a result of the transformation mechanism present in $ZrO_2$ containing ceramics.

The presence of SiC particles effectively inhibits $Al_2O_3$ grain growth in both materials (see Table 3 and Figs. 5 and 6). The results of $Al_2O_3$ grain size change with SiC

Table 2
Residual stresses, $\sigma$ (MPa), measured in $Al_2O_3$ grains from alumina and ZTA matrices as a function of SiC content

| Type of ceramic matrix | SiC content (wt%) | | | |
|---|---|---|---|---|
| | 0 | 10 | 20 | 30 |
| Alumina | −188.33 | +12.52 | +77.73 | +168.64 |
| ZTA | −115.94 | +44.14 | +143.61 | +155.47 |

[a] −refers to a residual compressive stress (for crystallographic plane *ab* of $\alpha$-$Al_2O_3$).
[b] + refers to a residual tensile stress.

Table 3
Mean $Al_2O_3$ grain size (μm) in alumina and ZTA matrices as a function of SiC content

| Type of ceramic matrix | SiC content (wt%) | | | |
|---|---|---|---|---|
| | 0 | 10 | 20 | 30 |
| Alumina | 4.67 ± 3.91 | 1.62 ± 0.78 | 0.96 ± 0.48 | 0.83 ± 0.27 |
| ZTA | 2.82 ± 1.19 | 1.55 ± 0.80 | 1.37 ± 0.58 | 1.26 ± 0.41 |

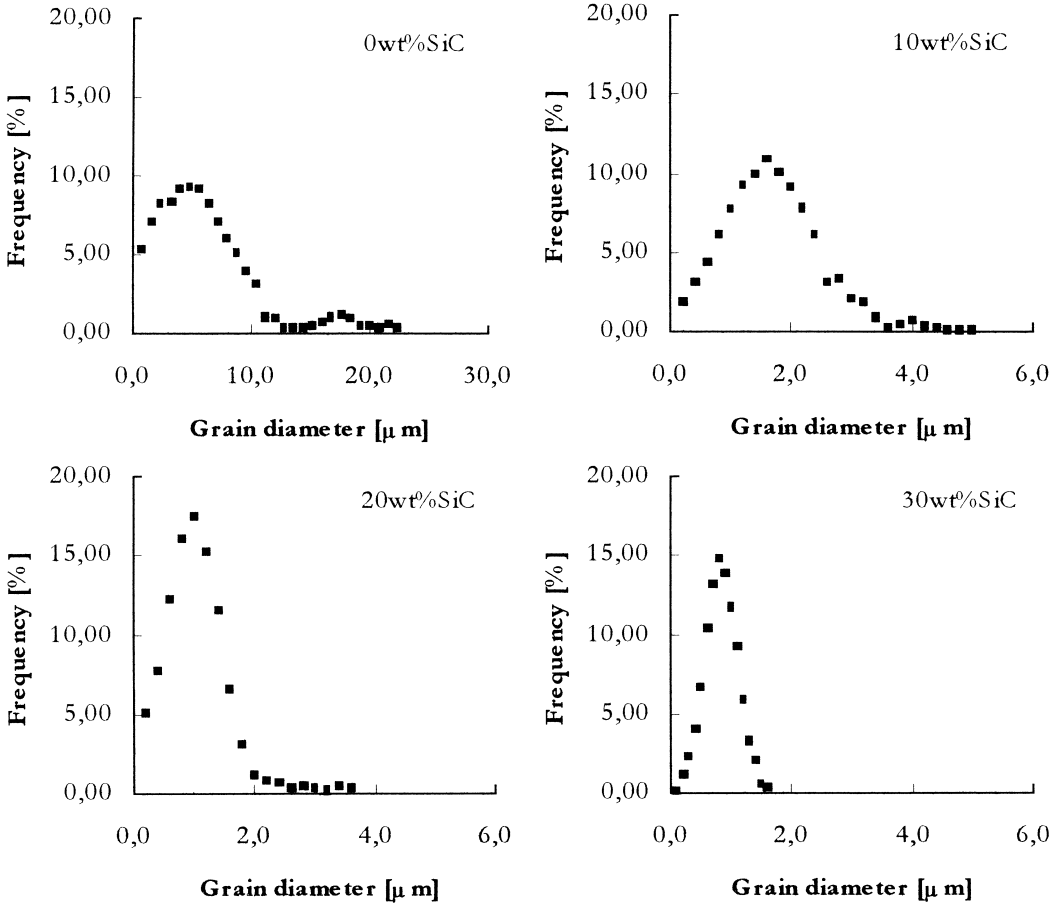


Fig. 5. $Al_2O_3$ grain size distribution in an alumina matrix as a function of the SiC particle content.

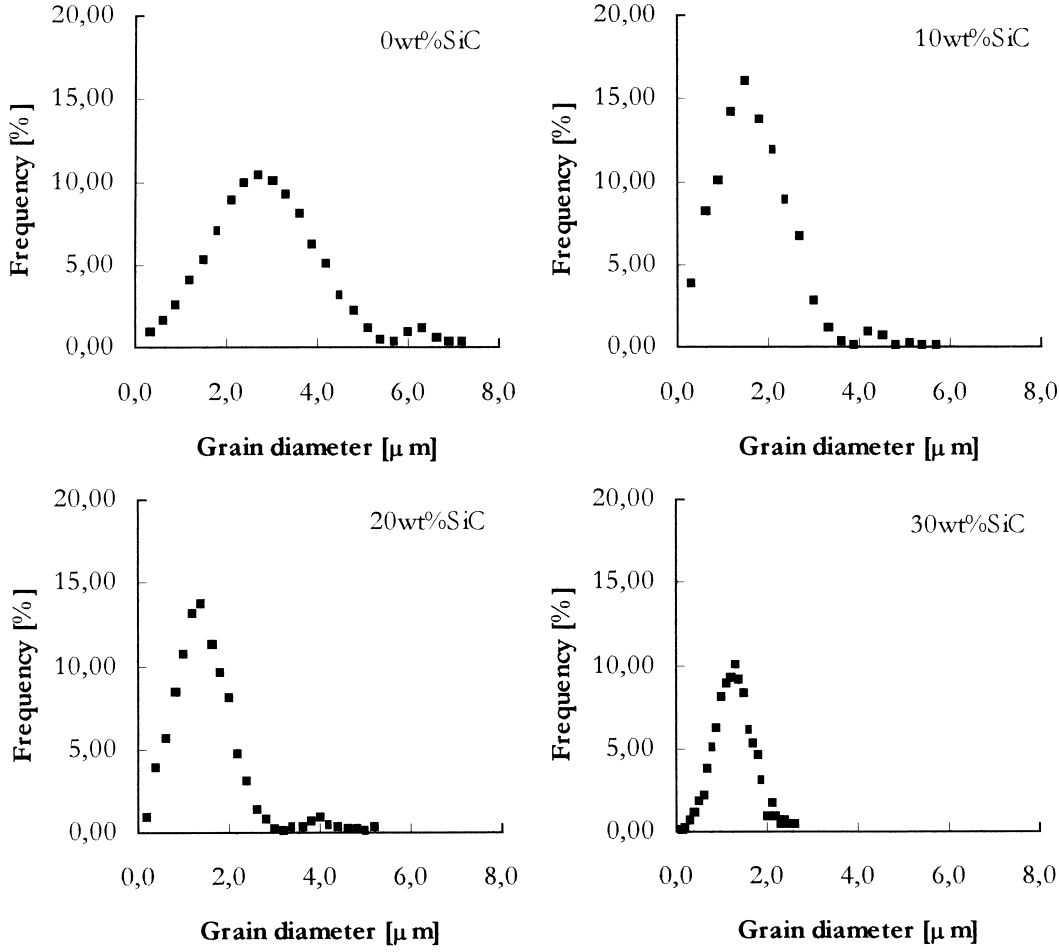


Fig. 6. $Al_2O_3$ grain size distribution in a ZTA matrix as a function of the SiC particle content.

content are intriguing in the context of the work of Chantikul et al.[16] They investigated the interrelationships between strength, crack-resistance characteristics and grain size for alumina ceramics in the grain size range of 2 to 80 μm. By deconvolution of strength-indentation data to *T*-curves they found that the toughness curves rise markedly especially for the coarser grain structures. For the $Al_2O_3$ grain sizes observed in our study, however, the slope angle of the toughness curves do not seem to be significant, which indicates a weak contribution of the grain size effect to the *R*-curve properties of the composites studied.

For verifying the contribution of $Al_2O_3$ grain size to the change of the *R*-curve properties of alumina and ZTA matrices with SiC particles added, alumina ceramics with different grain sizes were prepared and controlled crack growth experiments were performed. As can be seen from Table 4, for alumina ceramics the value of the slope parameter *a* strongly decreases with decreasing grain size. However, for the smallest grain size, the parameter *a* has still a significant value. This means that the change of the residual stresses caused by SiC presence can be regarded as the main factor responsible for the observed changes in *R*-curve behaviour of alumina and ZTA matrices.

Table 4
Linear coefficients *a* and *b* (from equation $y=ax+b$) for alumina ceramics as a function of $Al_2O_3$ grain size

| $Al_2O_3$ grain size (μm) | Linear coefficients | |
|---|---|---|
| | *a* | *b* |
| 2.3 ± 0.9 | 0.438 ± 0.189 | 3.173 ± 0.449 |
| 18.6 ± 8.9 | 0.665 ± 0.025 | 3.169 ± 0.076 |
| 39.7 ± 17.2 | 1.599 ± 0.034 | 0.798 ± 0.283 |
| 67.4 ± 29.4 | 1.885 ± 0.143 | 0.125 ± 0.267 |

The predicted and experimentally confirmed distribution of residual stress in the composites studied can be illustrated by a scheme shown in Fig. 7, where SiC particulates under compressive stress are immersed in a tensile stress of a ceramic matrix. Such a distribution indicates that the tensile stress in a matrix, acting perpendicularly to the crack plane, will promote extension of the crack over an interparticular region, $\lambda$-*d*, (see Fig. 8) and will decrease the stress intensity factor, $\Delta K_I$, of the composite according to Eq. (1) or (2). When a crack will

advance across the interparticulate region, the crack tip will meet the local compressive stress field generated outside a single SiC particle and changing as a function of distance according to Eq. (10) given by Selsing:[19]

$$\sigma_r = -2\sigma_o = P\left(\frac{R}{r}\right)^3 \tag{10}$$

where $\sigma_r$ is the radial and $\sigma_o$ the tangential component of the matrix stress, $P$, at the boundary of a spherical particle, $R$ is the radius of the particle and $r$ is the distance from the particle center. This local compressive microstress due to adjacent SiC particle can deflect a propagating crack and contributing this way in enhancing the toughness of the composite, as was observed in the composite studied and in layered ceramic composites described earlier.[13,15] The crack deflection model of Faber and Evans[20] predicts the toughness ratios of $K_{Ic}/K_{Im} = 1.12$ to 1.15 for uniformly distributed particles with particle volume fraction of $f_p = 0.1$ to 0.3. The decrease in the stress intensity factor, $\Delta K_I$, of the matrix due to the presence of tensile stress, obtained for a 30 wt% SiC content in an alumina matrix using Eq. (2), equals $\Delta K_I = 0.28$MPa $m^{1/2}$. The values of $q = \sigma_t = +168.64$ MPa (see Table 2), $\lambda = 2.07\mu$m (an average interparticle spacing, which was found from SEM photos) and $d = 1\mu$m (SiC particle size) were used in this evaluation. The resulting and measured fracture toughness of composites seems to be the sum of the contribution of the two, above mentioned, opposite mechanisms as a function of SiC particle content.

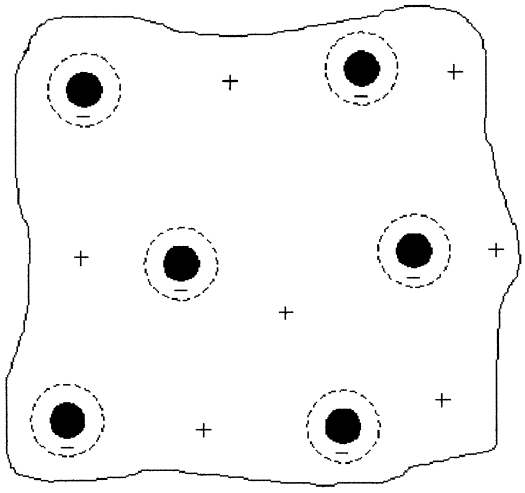

Fig. 7. Scheme of the thermal residual stress distribution in SiC particulate-reinforced alumina matrix composites.

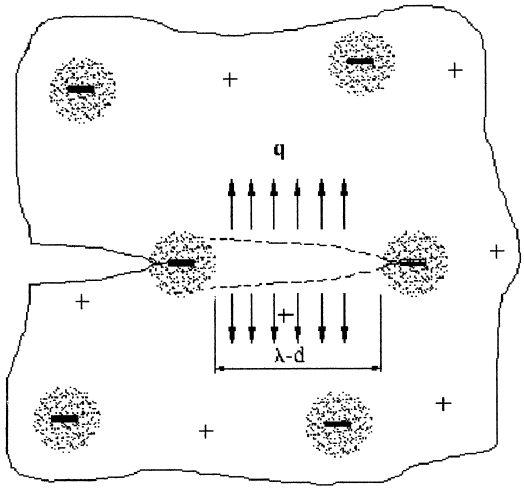


Fig. 8. Semi-infinite crack advances, λ, through matrix tensile region toward particle compressive region.

For some composites studied the tests of crack growth were performed also without removing the load. From these experiments the values of maximal stress intensity factor, $K_{Imax}$, resistance to crack initiation, $K_{Ii}$, and crack growth rate parameters $n$ and $A$ were obtained, which are listed in Table 5 and 6. As can be seen from Table 5, $K_{Imax}$ of the alumina matrix does not increase significantly with increasing SiC addition. However a strong increase of resistance to crack initiation ($K_{Ii}$) is observed. Also the rising values of the crack growth rate parameter $n$ show that an initiated crack will propagate with higher rate in an alumina matrix with SiC addition than in pure alumina.

In the case of the ZTA matrix the changes of $K_{Imax}$, resistance to crack initiation $K_{Ii}$ and crack growth rate

Table 5
Maximal stress intensity factor $K_{Imax}$, resistance to crack initiation $K_{Ii}$, and crack growth rate parameters n and $logA$ for an alumina matrix as a function of SiC content

| SiC content (wt%) | $K_{Imax}$ (MPa $m^{1/2}$) | $K_{Ii}$ (MPa $m^{1/2}$) | Crack growth rate parameters | |
|---|---|---|---|---|
| | | | $n$ | log$A$ |
| 0 | 4.78 ± 0.03 | 3.16 ± 0.06 | 8.17 ± 0.29 | −10.00 ± 0.17 |
| 10 | 4.92 ± 0.06 | 3.67 ± 0.03 | 28.83 ± 1.97 | −24.07 ± 1.36 |
| 20 | 4.90 ± 0.07 | 4.10 ± 0.24 | 36.20 ± 9.97 | −28.52 ± 6.08 |
| 30 | 4.86 ± 0.12 | 4.44 ± 0.19 | 44.03 ± 12.23 | −34.17 ± 8.41 |

Table 6
Maximal stress intensity factor $K_{Imax}$, resistance to crack initiation $K_{Ii}$, and crack growth rate parameters $n$ and log$A$ for ZTA matrix as a function of SiC content

| SiC content (wt%) | $K_{Imax}$ (MPa $m^{1/2}$) | $K_{Ii}$ (MPa $m^{1/2}$) | Crack growth rate parameters | |
|---|---|---|---|---|
| | | | $n$ | log$A$ |
| 0 | 5.08 ± 0.23 | 4.27 ± 0.05 | 23.77 ± 5.16 | −20.08 ± 2.17 |
| 10 | 5.14 ± 0.03 | 4.21 ± 0.07 | 21.27 ± 2.17 | −16.81 ± 2.53 |
| 20 | 5.40 ± 0.18 | 4.39 ± 0.01 | 23.10 ± 1.88 | −20.92 ± 1.59 |
| 30 | 5.23 ± 0.19 | 4.17 ± 0.03 | 16.91 ± 1.71 | −15.85 ± 1.70 |

Table 7
Bending strength, $\sigma$, and Young's modulus, $E$, of alumina and ZTA matrices as a function of SiC content

| SiC content (wt%) | Alumina matrix | | ZTA matrix | |
|---|---|---|---|---|
| | $\sigma$ (MPa) | $E$ (GPa) | $\sigma$ (MPa) | $E$ (GPa) |
| 0 | 355.9 ± 48.3 | 397.5 | 476.1 ± 29.5 | 356.6 |
| 10 | 384.2 ± 40.6 | 407.1 | 474.3 ± 14.4 | 359.6 |
| 20 | 428.9 ± 61.5 | 414.8 | 578.4 ± 53.5 | 371.6 |
| 30 | 439.6 ± 10.5 | 416.0 | 512.3 ± 54.9 | 374.3 |

parameters $n$ and $A$ are relatively small. However, a distinct increase of bending strength with SiC content was found for both matrices (Table 7). In contrast to the results of Levin et al.,[11] the observed increase in strength can not be attributed to a change of the alumina matrix fracture mode. Microscopic observation of crack paths points out that in a pure alumina the fracture mode is mostly intergranular, with transgranular fracture being partly present for grains larger than 15 μm. In alumina matrices with SiC grains the only mode found was intergranular fracture. The grain size measurements indicated (Figs. 5 and 6) that increasing SiC content, in both matrices, eliminates the small population of very large grains and this phenomenon can be responsible for the observed increase in strength. Another explanation comes from the model of Pezzotti et al.[18] describing a crack-closure micromechanism by local residual stresses, which proposes to explain the existence of a maximum in strength of $Al_2O_3/ZrO_2$ composites at moderate volume fractions of $Al_2O_3$. In our case the SiC particles are similarly in a strong compressive stress field which, due to equilibrium considerations, will produce locally high tension in the $Al_2O_3$ matrix. When two SiC particles are sufficiently close and placed on the opposite sides of the microcrack, the local residual microstresses can either shield the microcrack or, at least, delay its formation resulting in the observed strength increase.

## 4. Conclusions

The aim of this work was to determine the effect of the change in the residual stress state on $R$-curve properties of alumina and ZTA ceramics. To faciliate this, SiC particles, having a lower thermal expansion coefficient, were added to two different alumina matrices. Tests of controlled crack growth for both matrices having various SiC contents were performed. Data of $K_I = f(c)$ obtained in the range of the crack lengths studied were approximated by a linear equation of $y = ax + b$. As a result the slope parameter $a$ was used as a factor for describing the tendency of these ceramics to $R$-curve behaviour. A decreasing effect of SiC particles content on toughness-crack length dependence was found. The observed changes were related to measurements of residual stresses. It was found that an increasing content of SiC grains changed the residual stresses in both types of matrices from compressive to tensile. This in turn reduced the effectiveness of grain bridging and in consequence the value of slope parameter $a$. The smaller decrease of parameter $a$ with increasing SiC content observed in ZTA can probably be regarded as a result of the transformation mechanism present in a $ZrO_2$ containing alumina matrix. An increase of resistance to crack initiation and bending strength with increased SiC addition was also found for the studied ceramics.

## References


1. Bennison, S. J. and Lawn, B. R., Role of interfacial grain-bridging sliding friction in the crack-resistance and strength properties of non-transforming ceramics. *Acta. Metall.*, 1989, **37**(10), 2659–2671.
2. Chantikul, P., Bennison, S. J. and Lawn, B. R., Role of grain size in the strength and *R*-Curve properties of alumina. *J. Am. Ceram.Soc.*, 1990, **73**(8), 2419–2427.
3. Padture, N., Bennison, S. J., Runyan, J., Rodel, J., Chan, H. M. and Lawn, B. R., Flaw-tolerant alumina-aluminium titanate composites. In *Ceramic Transactions: Advanced Composite Materials*, ed. K. M. Nair. American Ceramic Society, Westerville, OH, 1991, pp. 715–721.
4. Stuart, M. Characterization and mechanical behaviour of the alumina–mullite system. M.S. thesis, Lehigh University, Bethlehem, PA, 1991.
5. Padture, N. T. and Chan, H. M., Improved flaw tolerance in alumina containing 1 vol% anorthite via crystallization of the intergranular glass. *J. Am. Ceram. Soc.*, 1982, **75**(7), 1870–1875.
6. Virkar, A. V. and Johnson, D. L., Fracture behaviour of $ZrO_2$–Zr Composites. *J. Am. Ceram. Soc.*, 1977, **60**(11–12), 514–519.
7. Taya, M., Hayashi, S., Kobayashi, A. S. and Yoon, H. S., Toughening of a particulate-reinforced ceramic-matrix composite by thermal residual stress. *J. Am. Ceram. Soc.*, 1990, **73**(5), 1382–1391.
8. Evans, A. G., Heuer, A. H. and Porter, D. L., The fracture toughness of ceramics. *Proc. Int. Conf. Fract.*, 1977, **4th**(I), 529–556.
9. Cutler, R. A. and Virkar, A. V., The effect of binder thickness and residual stress on the fracture toughness of cemented carbides. *J. Mater. Sci.*, 1985, **20**, 3557–3573.
10. Tada, H., Paris, P. C. and Irwin, G. R., *The Stress Analysis of Cracks Handbook*. Del Research Corp, Hellertown, PA, 1973 p.3,7.
11. Levin, I., Kaplan, W. D. and Brandon, D. G., Effect of SiC submicrometer particle size and content on fracture toughness of alumina–SiC nanocomposites. *J. Am. Ceram. Soc.*, 1995, **78**(1), 254–256.
12. Tomaszewski, H., Toughening effects in $Al_2O_3$–$ZrO_2$ system. *Ceramics Int.*, 1988, **14**, 117–125.
13. Tomaszewski, H., Strzeszewski, J. and Gebicki, W., The role of residual stresses in layered composites of Y–$ZrO_2$ and $Al_2O_3$. *J. Eur. Ceram. Soc.*, 1999, **19**, 255–262.
14. Fett, T. and Munz, D., Subcritical crack growth of macrocracks in alumina with *R*-Curve behaviour. *J. Am. Ceram. Soc.*, 1992, **75**(4), 958–963.
15. Tomaszewski, H., Weglarz, H., Boniecki, M. and Recko M., Effect of barrier layer thickness and composition on fracture

toughness of layered zirconia/alumina composites. *J. Mat. Sci.* submitted for publication.
16. Chantikul, P., Bennison, S. J. and Lawn, B. R., Role of grain size in the strength and *R*-Curve properties of alumina. *J. Am. Ceram. Soc.*, 1990, **73**(8), 2419–2427.
17. He, J. and Clarke, D. R., Determination of the piezospectroscopic coefficients for chromium-doped sapphire. *J. Am. Ceram. Soc.*, 1995, **78**(5), 1341–1359.
18. Pezzotti, G., Sergo, Sbaizero, O., Muraki, N., Meriani, S. and Nishida, T., Strengthening contribution arising from residual stresses in $Al_2O_3/ZrO_2$ composites: a piezo-spectroscopy investigation. *J. Eur. Ceram. Soc.*, 1999, **19**, 247–253.
19. Selsing, J., Internal stresses in ceramics. *J. Am. Ceram. Soc.*, 1961, **44**(8), 1419.
20. Faber, K. T. and Evans, A. G., Crack deflection processes — I. theory. *Acta Metall.*, 1983, **31**(4), 565–576.